Nanoscale

PAPER

View Article Online
View Journal

Cite this: DOI: 10.1039/d5nr04519c

Edge functionalization of graphyne nanoribbons for lithium-ion battery electrodes: a computational study

Raul Ekberg Dias and Alexandre Lopes de Magalhaes *

Lithium-ion batteries (LIBs) have become a vital part of the world's energy storage solutions over the past decades, mostly in the small electronics and electric vehicle markets. Lithium's high energy density and graphene's superior electronic properties make them a perfect combination for the most common LIBs used today. In recent years, other nanomaterials such as graphyne have emerged as highly promising candidates for innovative electrode designs. To explore this potential, the present study employs density functional theory (DFT) calculations to systematically investigate the structure and electronic properties of 56 unique graphyne compounds, evaluating their suitability as cathode materials for LIBs. A total of eight substituents were considered in this study, namely carbonyl, nitrile, nitro, carboxyl, trichloromethyl, trifluoromethyl, sulfeno, and dimethylamino groups. This study reveals that, among the functional groups analyzed, nitro and carbonyl groups consistently yielded the most significant enhancements in redox potential, achieving values as high as 5.0 V and 2.9 V, respectively. Other substituents did not impact the redox potential when compared to the pristine state with the exception of tetrasubstituted trifluoromethyl graphyne that reached a potential of 2.9 V. Moreover, the study demonstrates that the highest redox potentials in multi-substituted graphyne compounds were associated with locally distributed configurations, highlighting the benefits of controlled substitution within the graphyne framework.

Received 27th October 2025,
Accepted 6th January 2026

DOI: 10.1039/d5nr04519c

rsc.li/nanoscale

Introduction

The global transition from fossil fuels to "green" alternatives that are less aggressive to the environment, such as rechargeable batteries, solar, wind, tidal and others, has guided research to explore different materials and technologies to meet energy storage demands.[1] In the small portable electronics and electric vehicle fields, secondary lithium-ion battery (LIB) storage has been widely established because of its high volumetric and gravimetric energy densities, long storage lifetimes, limited self-discharge and other relevant properties.[2–4]

Two-dimensional (2D) carbon materials have emerged as prominent objects of study in the last two decades since the isolation of graphene in 2004 and later the synthesis of a graphdiyne film in 2010.[5,6] The lithium-ion battery (LIB) market adopted graphene-based electrodes into their cell designs because of their high electrical conductivity, thermal stability and low cost.[7–9] Other carbon allotropes have been considered as candidates in the development of LIBs because of their similarities with graphene and the promising higher theoretical capacity and higher carrier mobility that can lead to longer battery life and improved cell efficiency.[10–13]

Graphyne comprises sp and sp^2 hybridized carbons shaped into a flat repeating structure that forms a delocalized π system creating interesting electronic properties. The combination of differently hybridized carbon atoms in graphyne results in a higher band gap and lower atom density, which together contribute to a greater lithium storage capacity compared to graphene.[14] Graphynes are classified by the number of acetylenic linkages between their sp^2 hybridized carbons and the spatial arrangement of these atoms (Fig. 1), and their nomenclature follows the format X-graph-n-yne, where X is a prefix (such as α, β, or γ) that denotes the different ways the sp and sp^2 hybridized carbon atoms can be spatially combined, and n represents the number of acetylene groups in the unit cell. The ratio of sp and sp^2 hybridized carbon atoms within the network, along with the specific bonding configurations, can significantly influence key material properties such as electronic transport, aromaticity and other structural and functional characteristics.[15,16]

This study employed a γ-graphyne framework (Fig. 2), functionalized with all the specified substituents, and systematically evaluated the resulting structural and electronic pro-

LAQV/Requimte, Departamento de Química e Bioquímica, Faculdade de Ciências da Universidade do Porto, Rua do Campo Alegre, s/n, 4169-007 Porto, Portugal.
E-mail: almagalh@fc.up.pt, raulekberg@fc.up.pt; Tel: +351 220402504

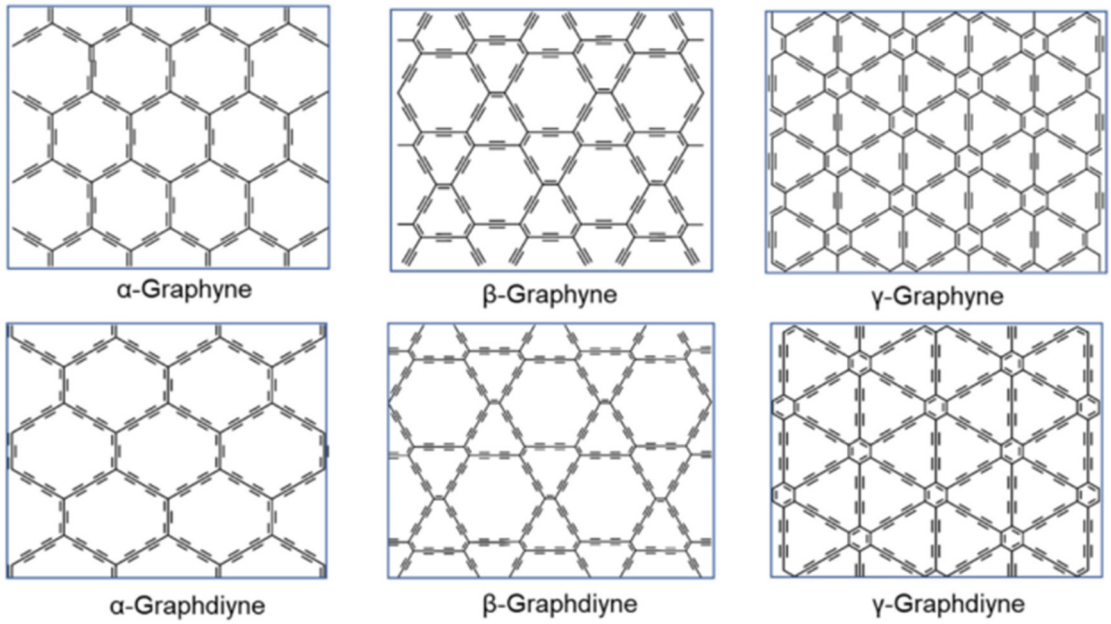

Fig. 1 Diagram of the graphene structure with the substituent sites enumerated (adapted from ref. 17).

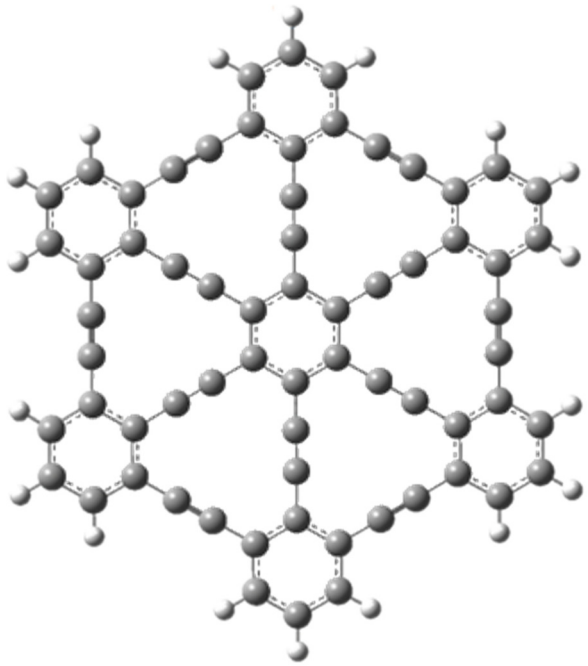

Fig. 2 Structure of pristine γ-graphyne.

perties. The γ-graphyne framework naturally forms a porous, triangular structure between its aromatic rings. These spaces are energetically favorable for adsorbing lithium ions, making them perfect for battery applications.[17] This high lithium storage capacity and excellent ion mobility of γ-graphyne make it a promising electrode material for LIBs.[18] Recent computational studies of more complex, multi-layered graphyne based structures, such as naphyne and pentagraphyne, have also demonstrated promising potential for lithium-ion battery applications.[19,20]

Computational details

All *ab initio* calculations were performed using the Gaussian 16 software package,[21] applying density functional theory (DFT) to compute the energy levels, redox potentials, and electron affinities of modeled carbon nanomaterials. The exchange–correlation energies were approximated using the global-hybrid MN15 functional developed by the Truhlar group,[22] in combination with the 6-31+G(d,p) basis set for improved accuracy. The MN15 functional is a highly parameterized hybrid *meta*-GGA functional that implicitly includes empirical dispersion corrections, improving its performance for van der Waals interactions and has already demonstrated reliability in previous related studies.[23] The key metric to compare these compounds in lithium-ion battery applications was their redox potentials, which were evaluated relative to the lithium electrode when paired with an organic cathode, as evidenced in eqn (1).

$$\Delta E^{\circ} = \left(-\frac{\Delta G^{\mathrm{red}}(R, \mathrm{sol})}{n_{\mathrm{e}} F} - E_{\mathrm{H}} \right) - E_{\mathrm{Li}} \quad (1)$$

In this context, E_{Li} represents the redox potential of the Li/Li^{+} electrode relative to the standard hydrogen electrode (SHE), which is −3.04 V,[24] while E_{H} denotes the absolute redox potential of hydrogen, valued at 4.44 V.[25] The term n_{e} corresponds to the number of electrons involved in the redox process, F is the Faraday constant, and $\Delta G^{\mathrm{red}}(S,\mathrm{sol})$ represents the Gibbs

free energy required to reduce the cathode in solution. It is well established that direct calculation of reduction energies in solution using DFT-derived energies of the two redox states often leads to inaccuracies.[26] To overcome this limitation,[26–28] the term $\Delta G^{red}(S,sol)$ was calculated using eqn (2), which is derived from the thermodynamic cycle depicted in Fig. 3:

$$\Delta G^{red}(R,sol) = \Delta G^{red}(R,gas) + \Delta G^{solv}(R^-) - \Delta G^{solv}(R) \quad (2)$$

where $\Delta G^{red}(R,gas)$ represents the Gibbs free energy of reduction in the gas phase, $\Delta G^{solv}(R^-)$ corresponds to the Gibbs free energy of solvation for the anionic state, and $\Delta G^{solv}(R)$ denotes the Gibbs free energy of solvation for the neutral state.

In the gas phase, frequency calculations of the normal vibrational modes were performed at the same level of theory for both the neutral and anionic states. For the solution phase, these calculations were carried out using the self-consistent reaction field (SCRF) method, employing the integral equation formalism variant of the polarizable continuum model (IEFPCM).[29] This approach models the molecule as being placed within a cavity embedded in a polarizable dielectric medium, which in turn influences its Hamiltonian. Custom solvent parameters were applied to simulate a mixture of ethylene carbonate (EC) and dimethyl carbonate (DMC), a common electrolyte blend in lithium-ion batteries (LIBs). EC provides a high dielectric constant and decomposes into a passivating layer that does not hinder battery performance, while DMC reduces the viscosity and melting point of the mixture.[30]

An 8 : 2 molar ratio of ethylene carbonate (EC) to dimethyl carbonate (DMC) was selected as the solvent for the solvation free energy calculations because electrolyte solutions containing more EC than DMC have been shown to enable a more reliable charge and discharge cycle,[31] and a thermodynamically stable electrolyte–ion complex.[32] The static dielectric constant was set to 62.43,[33] while the dynamic dielectric constant and solvent radius were set to 1.380 and 2.41 Å, respectively (see the SI).

The graphyne systems were modeled from a base γ-graphyne structure comprising 66 carbon atoms that have been previously studied.[23] This molecular model offers a good compromise between the quality of its predicted properties and the computational time needed to handle such large multi-substituted graphynes. Considering the electronic properties of graphyne-like structures, we selected a set of substituents spanning a wide range of inductive effects. Due to limited literature data on promising groups and based on previous studies,[23] the eight substituents studied were carbonyl (–O), nitrile (–CN), nitro ($–NO_2$), carboxyl (–COOH), trichloromethyl ($–CCl_3$), trifluoromethyl ($–CF_3$), sulfeno (–SOH) and dimethylamino ($–N(CH_3)_2$) groups. These compounds were modeled to account for different positional isomers in two different configurations. The first, labeled Uniformly Distributed, featured substituents added uniformly and symmetrically to the edges of the base γ-graphyne nanoribbon. The second, designated Locally Distributed, involved the continuous addition of substituents at equivalent, localized sites within the molecular framework (Fig. 4). This was done to evaluate how the position of the substituents relative to each other in the carbon framework can impact the redox potential.

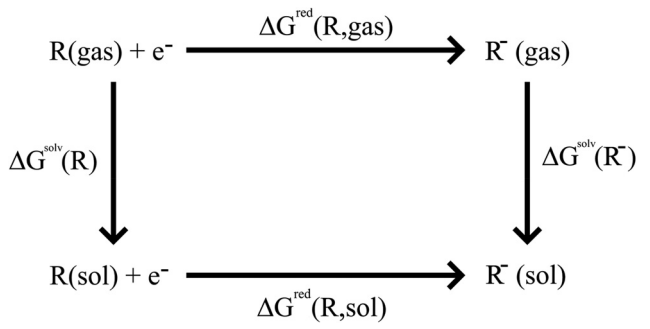

Fig. 3 Diagram of the thermodynamic cycle adopted to calculate the free energy of reduction of cathodes in solution.

Results and discussion

All molecular structures were fully optimized at the MN15/6-31+G(d,p) DFT level of theory, with the graphyne carbon framework remaining planar and no significant geometric distortions observed in the substituents. The calculated redox potentials and electron affinities of all 56 compounds have been split into three different groups, namely monosubstituted, multi-substituted uniformly, and multi-substituted locally, as depicted in Tables 1–3, respectively. For each substituent group, the sequential substitution into the graphyne based pattern produced seven unique compounds, which are schematized in Fig. 4 and labeled with a reference notation in the first column of these tables. In this context, the identification of these compounds was based on three key structural features: the number of substituents, their spatial configuration, and the nature of the substituents. Each compound is denoted by the prefix G, representing the graphyne framework, followed by the letter *m*, *u* or *l*, indicating the substitution pattern, respectively, monosubstitution, multi-substitution with the uniform configuration, or multi-substitution with the local configuration. For multi-substituted compounds, the configuration symbol is followed by the number of substituents and the substituent label. For example, Gl3NO2 refers to the graphyne derivative with three nitro groups placed locally to the base structure. In this notation, G alone stands for the pristine graphyne without any substituents.

The redox potentials of the functionalized compounds were compared to the 2.1 V redox potential of pristine γ-graphyne, which served as the baseline. Among the monosubstituted compounds, only those with nitro and carbonyl groups, identified as $GmNO_2$ and GmO, show significant increases in their values, as 2.5 V and 3.5 V, respectively. In fact, the remarkable performance of the latter substituent has previously been demonstrated in the context of carbonyl edge-functionalization of both graphene and graphyne.[23,34]

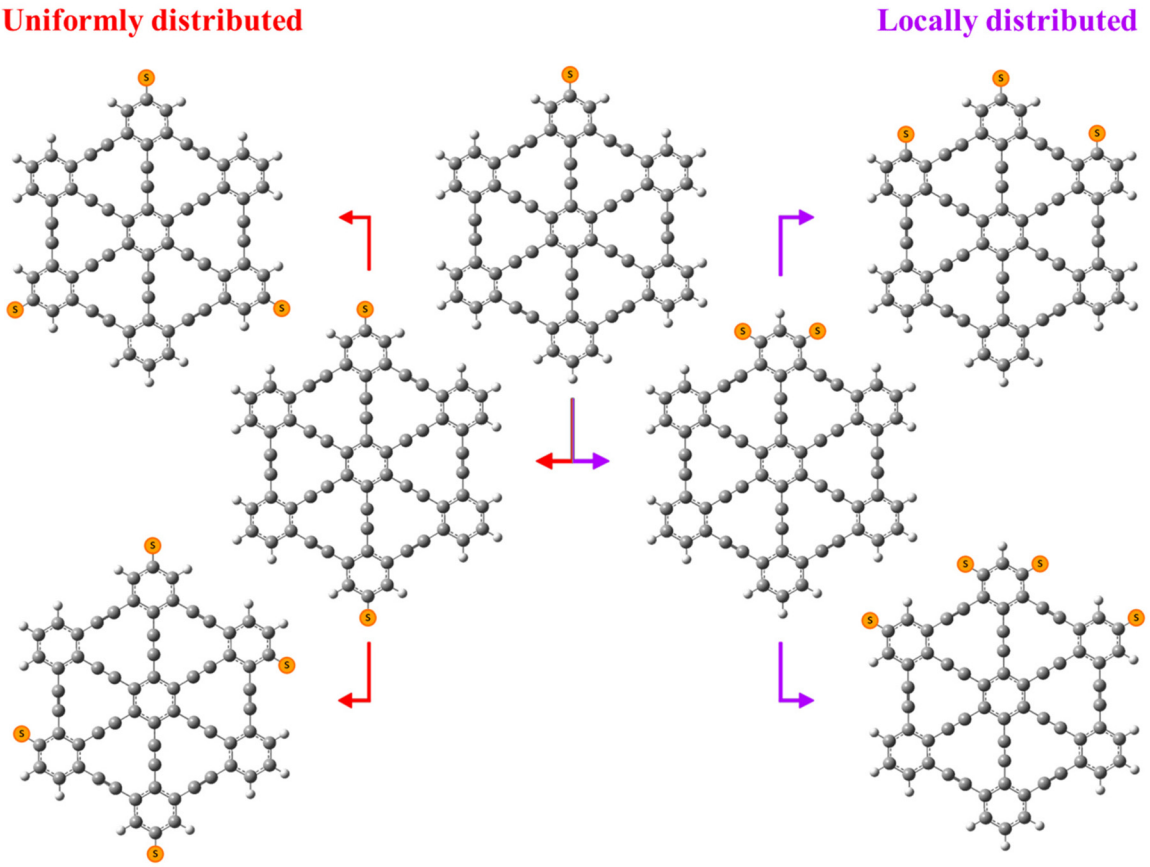

Fig. 4 Diagram of the two configurations adopted for multi-substituted compounds, uniformly distributed (red) and locally distributed (purple), where the substituent sites are indicated in orange.

Table 1 Redox potential and electron affinity for monosubstituted graphynes

Monosubstituted			
Identifier	Substituent	Redox potential (V *vs.* Li/Li^+)	Electron affinity (eV)
G	No substituent	2.1	−1.89
GmCOOH	(–COOH)	2.2	−2.28
GmNO2	($–NO_2$)	2.5	−2.36
GmCN	(–CN)	2.2	−2.20
GmSOH	(–SOH)	2.1	−2.26
GmCF3	($–CF_3$)	2.2	−2.02
GmCCl3	($–CCl_3$)	2.2	−2.10
GmNMe2	($–N(CH_3)_2$)	2.1	−1.80
GmO	(–O)	3.5	−3.23

In general, the successive addition of the same substituent slightly increases the redox potentials. This effect is especially pronounced in the presence of nitro and, most notably, carbonyl functional groups. Although the trifluoromethyl-substituted graphyne achieved a redox potential of 2.9 V, comparable to that of the nitro group, the remaining compounds in its family did not follow a consistent trend in redox potential. This inconsistency makes it difficult to identify it as a suitable

Table 2 Redox potential and electron affinity for multi-substituted uniformly distributed graphynes

Identifier	Number of substituents	Redox potential (V *vs.* Li/Li^+)	Electron affinity (eV)
G	No substituent	2.1	−1.89
Gu2COOH	2 (–COOH)	2.3	−2.28
Gu3COOH	3 (–COOH)	2.2	−2.46
Gu4COOH	4 (–COOH)	2.3	−2.10
Gu2NO2	2 ($–NO_2$)	2.6	−2.65
Gu3NO2	3 ($–NO_2$)	2.3	−2.74
Gu4NO2	4 ($–NO_2$)	2.6	−2.98
Gu2CN	2 (–CN)	2.3	−2.45
Gu3CN	3 (–CN)	2.3	−2.55
Gu4CN	4 (–CN)	2.4	−2.75
Gu2SOH	2 (–SOH)	2.1	−2.09
Gu3SOH	3 (–SOH)	2.1	−2.08
Gu4SOH	4 (–SOH)	2.1	−2.13
Gu2CF3	2 ($–CF_3$)	2.2	−2.28
Gu3CF3	3 ($–CF_3$)	2.4	−2.36
Gu4CF3	4 ($–CF_3$)	2.3	−2.52
Gu2CCl3	2 ($–CCl_3$)	2.2	−2.25
Gu4CCl3	4 ($–CCl_3$)	2.3	−2.48
Gu2NMe2	2 ($–N(CH_3)_2$)	2.0	−1.71
Gu3NMe2	3 ($–N(CH_3)_2$)	1.9	−1.50
Gu4NMe2	4 ($–N(CH_3)_2$)	2.0	−1.61
Gu2O	2 (–O)	3.8	−3.97
Gu3O	3 (–O)	2.7	−2.91
Gu4O	4 (–O)	4.8	−5.38

Table 3 Redox potential and electron affinity for multi-substituted locally distributed graphynes

Identifier	Number of substituents	Redox potential (V *vs.* Li/Li^+)	Electron affinity (eV)
G	No substituent	2.1	−1.89
Gl2COOH	2 (–COOH)	2.2	−2.10
Gl3COOH	3 (–COOH)	2.2	−2.27
Gl4COOH	4 (–COOH)	2.2	−2.39
Gl2NO2	2 ($–NO_2$)	2.0	−2.59
Gl3NO2	3 ($–NO_2$)	2.6	−2.62
Gl4NO2	4 ($–NO_2$)	2.9	−2.98
Gl2CN	2 (–CN)	2.3	−2.45
Gl3CN	3 (–CN)	2.3	−2.48
Gl4CN	4 (–CN)	2.4	−2.71
Gl2SOH	2 (–SOH)	2.1	−1.98
Gl3SOH	3 (–SOH)	2.1	−2.09
Gl4SOH	4 (–SOH)	2.1	−2.08
Gl2CF3	2 ($–CF_3$)	2.2	−2.11
Gl3CF3	3 ($–CF_3$)	2.3	−2.30
Gl4CF3	4 ($–CF_3$)	2.9	−2.44
Gl2CCl3	2 ($–CCl_3$)	2.2	−2.11
Gl3CCl3	3 ($–CCl_3$)	2.2	−2.29
Gl4CCl3	4 ($–CCl_3$)	2.3	−2.40
Gl2NMe2	2 ($–N(CH_3)_2$)	2.1	−1.91
Gl3NMe2	3 ($–N(CH_3)_2$)	2.2	−1.81
Gl4NMe2	4 ($–N(CH_3)_2$)	2.0	−1.69
Gl2O	2 (–O)	4.1	−3.87
Gl3O	3 (–O)	2.9	−2.90
Gl4O	4 (–O)	5.0	−5.23

candidate, as the desired properties depend heavily on the precise number and spatial arrangement of substituents. The only exception was observed in the case of functionalization with dimethylamino groups, where the configuration involving three such groups uniformly distributed (Gu3NMe2) exhibited the lowest redox potential among all graphynes studied, decreasing to 1.9 V relative to the pristine state.

Based on the data presented in Fig. 5, no significant differences are observed between the trends of the uniform and the local configurations. However, a preference for the latter one is suggested, especially with the four substitutions with nitro, trifluoromethyl, and carbonyl groups; the compounds Gl4NO2, Gl4CF3, and Gl4O, with four locally distributed functionalizations, reached the highest values for the calculated redox potentials, 2.9, 2.9, and 5.0, respectively, when compared with the three equivalent cases of four uniform functionalizations, namely Gu4NO2, Gu4CF3, and Gu4O, which exhibited the values of 2.6, 2.3, and 4.8, respectively. The only exception to this trend was the uniformly disubstituted nitrographyne Gu2NO2, which had a higher redox potential of 2.6 V, while its locally substituted counterpart, Gl2NO2, showed a lower redox potential of 2.0 V.

An evident characteristic from the analysis of uniform multi-substitution is the reduction of redox potentials when three substituents are used, particularly with carbonyl groups. This observation indicates a potential periodic oscillation in electronic properties, which may be attributed to an even-odd effect, a phenomenon previously reported in molecular carbon systems.[35,36] However, due to the limited sample size in the present study, this conclusion remains tentative, and additional calculations are planned in future work to further explore the existence of this effect.

In Fig. 5, a gap is noticeable within the group of compounds bearing three uniformly distributed substituents, as well as only two entries in Table 2 under the trichloromethyl section. The missing data point corresponds to the trisubstituted trichloromethyl graphyne, for which frequency calculations failed to converge despite multiple attempts.

The electrostatic potential maps (ESP maps) were generated to assess the influence of functionalization on the electron distribution within the carbon framework and the corresponding

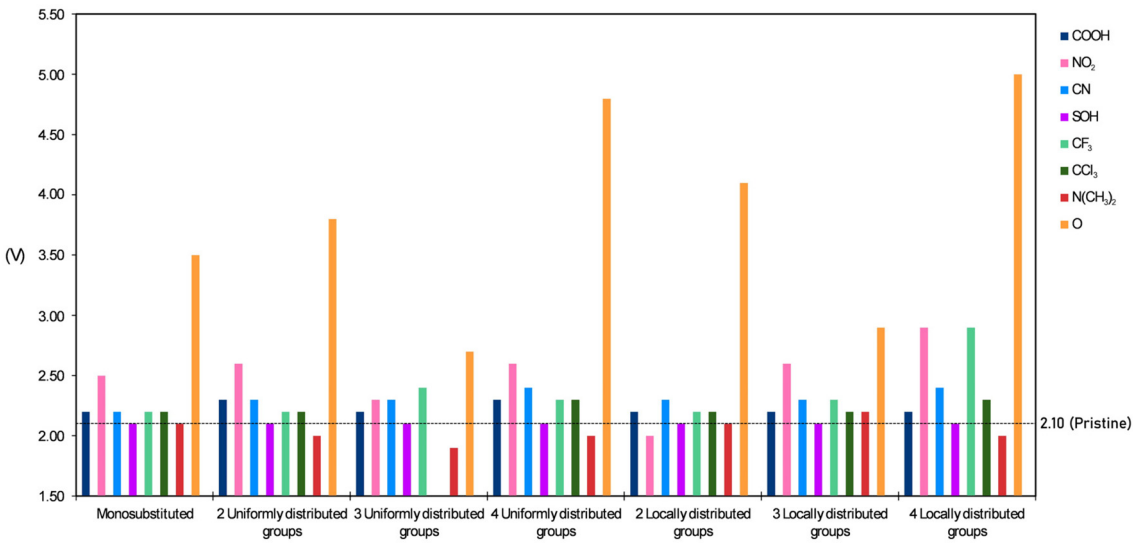

Fig. 5 Redox potential data for the graphyne compounds grouped by substituent configuration. The baseline for comparison is the pristine line crossing the bars with a value of 2.10 V.

associated substituents. Fig. 6 depicts the ESP maps of pristine γ-graphyne (A) and all the compounds functionalized with carbonyl groups, which were selected as representative examples due to their exceptionally high redox potentials. Furthermore, ESP maps were generated for all other substituted graphynes (see Fig. S1). A glance at Fig. 6 reveals that all substitutions lead to a withdrawal of electron density from the central region of the carbon framework when compared with the case of pristine γ-graphyne. The magnitude of this effect increases with the number of added substituents in both the local and uniform configurations. When comparing the two functionalization configurations with an equal number of substituents, it becomes evident that local multi-substitutions slightly enhance electron-withdrawing effects. This leads to the formation of larger regions of positive electrostatic potential, spatially separated from the negatively charged carbonyl groups. This might favor the electron affinity and, consequently, the process represented by the $\Delta G^{red}(R,gas)$ term in eqn (2), which results in higher redox potentials. Furthermore, in both configurations, the transition from two to three substituents, specifically from cases C and D to E and F, does not lead to pronounced changes in the electrostatic potential. This observation may be associated with the decrease in redox potential previously noted for the latter two compounds.

The performance of batteries is governed by a broad range of factors, from the chemical composition of materials to their physical architecture and operating conditions.[37] Among these, ion diffusion is a critical parameter, and the electrostatic potential profile of the electrode is expected to exert a significant influence on this process. To gain preliminary insights into this aspect, we calculated lithium-ion binding energies for all graphyne derivatives using the same DFT level of theory, as detailed in the SI.

All optimized geometries place the lithium ion above the center of the ring formed by acetylene bonds, at an average distance of 1.08 Å, with no perceptible distortions in the graphyne

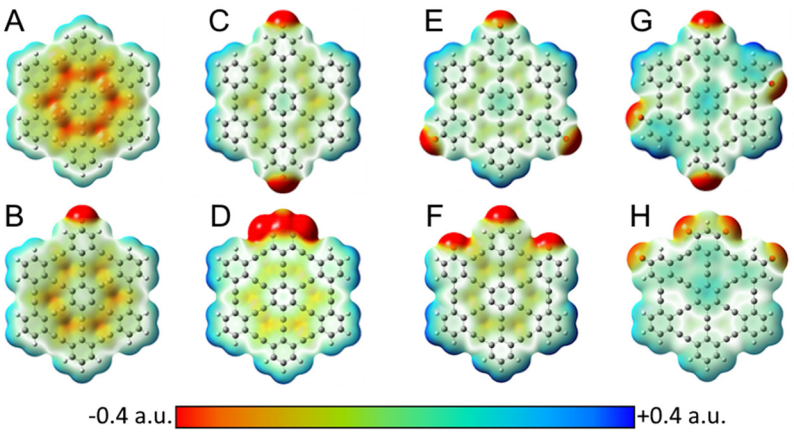

Fig. 6 Colored electrostatic potential maps on an isodensity surface of 0.001 a.u. of G (A), GmO (B), Gu2O (C), Gl2O (D), Gu3O (E), Gl3O (F), Gu4O (G), and Gl4O (H) compounds. The atoms represented are carbon (grey), hydrogen (white) and oxygen (red).

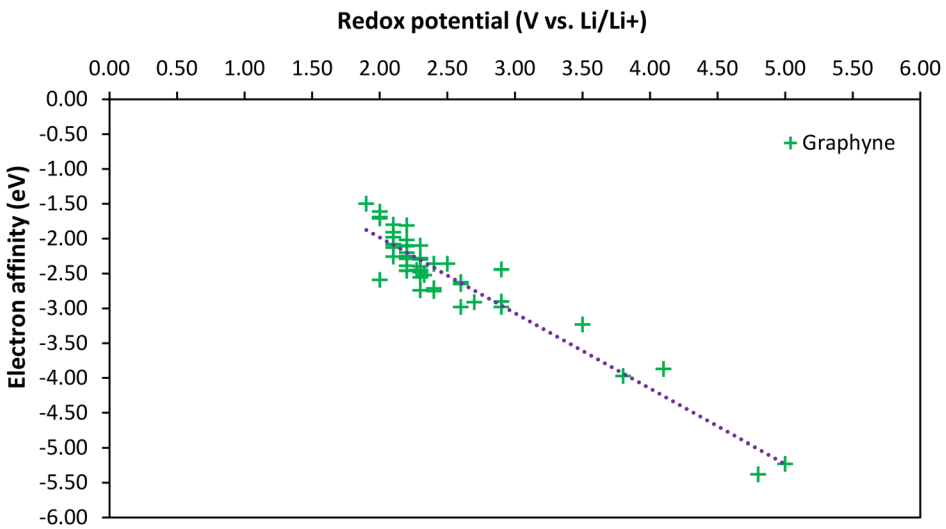

Fig. 7 Linear correlation between redox potential and electron affinity in the graphyne compounds.

framework. In general, all the functionalization with electron-withdrawing substituents resulted in weaker interactions compared to the pristine graphyne, which exhibits an interaction energy of −2.81 eV and serves as the reference. This trend is expected, as substituents with the negative inductive effect withdraw electron density from the carbon framework, as evidenced by the electrostatic potential maps, thereby weakening the interaction with the positively charged lithium ion. In contrast, the dimethylamino substituent, which exerts a slight electron-donating effect, enhances the interaction with the lithium ion and yields a more negative ΔE_{bind} value. Interestingly, this substituent also corresponds to the lowest redox potential among the studied cases, whereas carbonyl and nitro groups, despite having redox potentials markedly distinct from the others, do not exhibit significantly different interaction energies. Therefore, establishing a direct correlation between redox potential and ΔE_{bind} remains challenging in the present work and further studies are planned. Nevertheless, we anticipate that the latter factor may influence ion mobility across the electrode surface and, consequently, impact overall battery performance.

Previous studies have reported a strong correlation between electron affinities and redox potentials.[38,39] This relationship is expected, given that electron affinity is directly associated with the term $\Delta G^{red}(R,gas)$ in eqn (2), which represents the change in free energy when a neutral graphyne-based compound captures an electron. The data collected with the compounds of this work show a remarkable linear correlation between electron affinity and redox potentials, as depicted in Fig. 7, with a linear correlation coefficient of 0.8999.

Furthermore, the linear relationship observed between the two parameters arises naturally from eqn (1) and (2). This correlation plays a critical, albeit indirect, role in estimating redox potentials through the thermodynamic cycle illustrated in Fig. 3. It enables a significant simplification of the computational process, making theoretical predictions considerably more efficient compared to calculations involving solvent-dependent redox potentials. The simplified approach adopted in this study has demonstrated, in most cases, a reduction of approximately 50% in computation time.

Conclusions

In this work, we extended previous computational studies on the edge functionalization of carbon-based two-dimensional materials to evaluate and optimize their suitability as electrode materials in lithium-ion batteries. Eight chemically distinct substituents were employed in mono- or multi-substitution schemes along the edges of γ-graphyne nanoribbon models, configured in either local or uniform distributions. A total of 56 functionalized models were generated, and their redox potentials relative to the lithium electrode were computed using density functional theory at the DFT/MN15/6-31+G(d,p) level.

The data indicate that functionalization of graphyne with carbonyl and nitro groups resulted in the most significant enhancements in redox potential, reaching values up to 5.0 V and 2.9 V, respectively. These findings suggest that such substituents are promising candidates for the development of lithium-ion batteries requiring higher operational potentials. The surface charge analysis shows that compounds with higher redox potentials tend to have their partial charges more evenly spread across the carbon framework, while most of the negative charge sits on the substituents. This study also reveals a slight advantage in adopting a local multi-functionalization strategy, wherein substituents are spatially concentrated, compared to uniform configurations where substituents are evenly distributed along the edge of the nanoribbon model. Additionally, the observed linear correlation between redox potential and electron affinity offers a practical framework for preliminary screening of potential substituents using broader, computationally less intensive methods prior to engaging in more detailed calculations.

Author contributions

Raul E. Dias: conceptualization, investigation, methodology, and writing – original draft. Alexandre L. Magalhaes: data curation, writing – review and editing, and supervision.

Conflicts of interest

The authors declare that they have no known competing financial interests or personal relationships that could have appeared to influence the work reported in this paper.

Data availability

The data supporting this article have been included as part of the supplementary information (SI). Supplementary information is available. See DOI: https://doi.org/10.1039/d5nr04519c.

Acknowledgements

This work received financial support from the PT national funds (FCT/MECI, Fundação para a Ciência e Tecnologia and Ministério da Educação, Ciência e Inovação) through the project UID/50006/2025 (https://doi.org/10.54499/UID/50006/2025) – Laboratório Associado para a Química Verde – Tecnologias e Processos Limpos.

References

1 R. Mukherjee, R. Krishnan, T.-M. Lu and N. Koratkar, *Nano Energy*, 2012, **1**, 518–533.
2 Y. Nishi, *J. Power Sources*, 2001, **100**, 101–106.

3 K. S. Novoselov, A. K. Geim, S. V. Morozov, D. Jiang, Y. Zhang, S. V. Dubonos, I. V. Grigorieva and A. A. Firsov, *Science*, 2004, **306**, 666–669.
4 C. Peng, L. Kong, Y. Li, H. Fu, L. Sun, Y. Feng and W. Feng, *Sci. China Mater.*, 2021, **64**, 1367–1377.
5 J. M. Tarascon and M. Armand, *Nature*, 2001, **414**, 359–367.
6 G. Li, Y. Li, H. Liu, Y. Guo, Y. Li and D. Zhu, *Chem. Commun.*, 2010, **46**, 3256–3258.
7 J. Hou, D. Wang, M. Chao, L. Zhang, H. Liu and Y. Zhao, *Chem. Commun.*, 2024, **60**, 1908–1911.
8 S. Li, K. Wang, G. Zhang, S. Li, Y. Xu, X. Zhang, X. Zhang, S. Zheng, X. Sun and Y. Ma, *Adv. Funct. Mater.*, 2022, **32**, 2200796.
9 H. Geng, Y. Peng, L. Qu, H. Zhang and M. Wu, *Adv. Energy Mater.*, 2020, **10**, 1903030.
10 J. Chen, J. Xi, D. Wang and Z. Shuai, *J. Phys. Chem. Lett.*, 2013, **4**, 1443–1448.
11 H. Du, H. Yang, C. Huang, J. He, H. Liu and Y. Li, *Nano Energy*, 2016, **22**, 615–622.
12 S. Gong, S. Wang, J. Liu, Y. Guo and Q. Wang, *J. Mater. Chem. A*, 2018, **6**, 12630–12636.
13 L. Zhao, Y. Jiang, J. Hao, H. Wei, W. Zheng and L. Mao, *Sci. China: Chem.*, 2019, **62**, 1414–1420.
14 C. Sun and D. J. Searles, *J. Phys. Chem. C*, 2012, **116**, 26222–26226.
15 J. Yun, H. An, R. Huang, M. Guo, Y. Zhang and P. Kang, *IEEE Trans. Electron Devices*, 2020, **67**, 2529–2535.
16 J. Jusélius and D. Sundholm, *Phys. Chem. Chem. Phys.*, 2001, **3**, 2433–2437.
17 J. Li and Y. Han, *Giant*, 2023, **13**, 100140.
18 H. Zhang, M. Zhao, X. He, Z. Wang, X. Zhang and X. Liu, *J. Phys. Chem. C*, 2011, **115**, 8845–8850.
19 N. Barman, H. Dua and U. Sarkar, *Appl. Surf. Sci.*, 2025, **682**, 161649.
20 J. Deb, R. Ahuja and U. Sarkar, *ACS Appl. Nano Mater.*, 2022, **5**, 10572–10582.
21 M. J. Frisch, G. W. Trucks, H. B. Schlegel, G. E. Scuseria, M. A. Robb, J. R. Cheeseman, G. Scalmani, V. Barone, G. A. Petersson, H. Nakatsuji, X. Li, M. Caricato, A. V. Marenich, J. Bloino, B. G. Janesko, R. Gomperts, B. Mennucci, H. P. Hratchian, J. V. Ortiz, A. F. Izmaylov, J. L. Sonnenberg, D. Williams-Young, F. Ding, F. Lipparini, F. Egidi, J. Goings, B. Peng, A. Petrone, T. Henderson, D. Ranasinghe, V. G. Zakrzewski, J. Gao, N. Rega, G. Zheng, W. Liang, M. Hada, M. Ehara, K. Toyota, R. Fukuda, J. Hasegawa, M. Ishida, T. Nakajima, Y. Honda, O. Kitao, H. Nakai, T. Vreven, K. Throssell, J. A. Montgomery Jr., J. E. Peralta, F. Ogliaro, M. J. Bearpark, J. J. Heyd, E. N. Brothers, K. N. Kudin, V. N. Staroverov, T. A. Keith, R. Kobayashi, J. Normand, K. Raghavachari, A. P. Rendell, J. C. Burant, S. S. Iyengar, J. Tomasi, M. Cossi, J. M. Millam, M. Klene, C. Adamo, R. Cammi, J. W. Ochterski, R. L. Martin, K. Morokuma, O. Farkas, J. B. Foresman and D. J. Fox, *Gaussian 16 (Rev. C.01)*, Gaussian, Inc., Wallingford CT, 2016.
22 H. S. Yu, X. He, S. L. Li and D. G. Truhlar, *Chem. Sci.*, 2016, **7**, 5032–5051.
23 R. E. Dias and A. L. Magalhaes, *Comput. Theor. Chem.*, 2024, **1233**, 114494.
24 P. W. Atkins, *Shriver & Atkins' inorganic chemistry*, Oxford University Press, Oxford, 2010.
25 S. Trasatti, *Pure Appl. Chem.*, 1986, **58**, 955–966.
26 P. Winget, C. J. Cramer and D. G. Truhlar, *Theor. Chem. Acc.*, 2004, **112**, 217–227.
27 P. Winget, E. J. Weber, C. J. Cramer and D. G. Truhlar, *Phys. Chem. Chem. Phys.*, 2000, **2**, 1231–1239.
28 C. Y. Go, G. S. Jeong and K. C. Kim, *iScience*, 2019, **21**, 206–216.
29 G. Scalmani and M. J. Frisch, *J. Chem. Phys.*, 2010, **132**, 114110.
30 K. Xu, *Chem. Rev.*, 2004, **104**, 4303–4418.
31 J. Y. Kim, D. O. Shin, T. Chang, K. M. Kim, J. Jeong, J. Park, Y. M. Lee, K. Y. Cho, C. Phatak, S. Hong and Y.-G. Lee, *Electrochim. Acta*, 2019, **300**, 299–305.
32 O. Borodin and G. D. Smith, *J. Phys. Chem. B*, 2009, **113**, 1763–1776.
33 R. Naejus, D. Lemordant, R. Coudert and P. Willmann, *J. Chem. Thermodyn.*, 1997, **29**, 1503–1515.
34 S. Kim, K. C. Kim, S. W. Lee and S. S. Jang, *Phys. Chem. Chem. Phys.*, 2016, **18**, 20600–20606.
35 F. Crépin, H. Hettmansperger, P. Recher and B. Trauzettel, *Phys. Rev. B: Condens. Matter Mater. Phys.*, 2013, **87**, 195440.
36 T. Kawakami, T. Nomura and M. Koshino, *Phys. Rev. B*, 2020, **102**, 115421.
37 R. Khalid, A. Shah, M. Javed and H. Hussain, *RSC Adv.*, 2025, **15**, 15951–15998.
38 Y. Zhu, K. C. Kim and S. S. Jang, *J. Mater. Chem. A*, 2018, **6**, 10111–10120.
39 R. Jinnouchi and A. B. Anderson, *J. Phys. Chem. C*, 2008, **112**, 8747–8750.

